Control of Electronic and Magnetic Coupling via Bridging Ligand Geometry in a Bimetallic Ytterbocene Complex

Christin N. Carlson,[†] Brian L. Scott,[§] Richard L. Martin,[‡] Joe D. Thompson,[§] David E. Morris,*,[§] and Kevin D. John*,[†]

Chemistry, Theory, and Materials Physics Applications Divisions, Los Alamos National Laboratory, Los Alamos, New Mexico 87545

The ligand 1-methyl-3,5-bis(2,2′:6′,2′′-terpyridin-4′-yl)benzene has been employed in the synthesis of a new bimetallic ytterbocene complex [(Cp*)$_2$Yb](1-methyl-3,5-bis(2,2′:6′,2′′-terpyridin-4′-yl)benzene)[Yb(Cp*)$_2$] (**1**) and the doubly oxidized congener [**1**]$^{2+}$ in an attempt to determine the impact of the bridging ligand geometry on the magnetic/electronic properties as compared to the previously reported 1,4-analog [(Cp*)$_2$Yb](1,4-di(terpyridyl)benzene)[Yb-(Cp*)$_2$] (**2**). Electrochemical, electronic, and magnetic data provide compelling evidence that the 1,3-geometry associated with the bridging ligand of **1** has done an effective job of inhibiting electronic communication between metal centers and magnetic coupling of spin carriers at room temperature as compared to **2**. In fact, the physical data associated with **1** are quite similar to those reported for the monometallic analog (Cp*)$_2$Yb(tpy) (**3**). In particular, the f–f profile of [**1**]$^{2+}$ is nearly identical to that of [**3**]$^+$ in its spectral features but with an almost exact doubling of the intensities. Further, the electronic coupling between metal centers as manifested in the potential separation between metal-based reduction waves has for the first time in these bimetallic ytterbocene complexes been found to go to zero for **1**. Thus, the linkage isomerism at the phenyl coupling unit has induced a change in the ground-state electronic configuration from the singlet dianion-bridged (4f)^{13}(π*)^2(4f)^{13} state found in **2** to the diradical-bridged (4f)^{13}(π_A*)^1(π_B*)^1(4f)^{13} state in **1**. This diradical formulation on the bridging ligand in **1** is supported by DFT calculations for the uncomplexed doubly reduced ligand that indicate the ground-state configuration is a singlet diradical state with the triplet-diradical state lying to slightly higher energy. Magnetic characterization of **1** is most consistent with the behavior previously observed for monometallic analogs such as **3**, and there is no evidence of long-range magnetic ordering such as that observed for **2**. In addition, X-ray crystallographic characterization of **1** represents the first case of a structurally characterized 2:1 metal-to-ligand adduct of the 1,3-bis(tpy) framework.

Introduction

Previous efforts in our group and others have focused on systematic characterization of the internal charge-transfer process that exists in monometallic[1−3] and bimetallic[4−6]

ytterbocene complexes of polypyridyl ligands with the aim of understanding magnetic/electronic coupling that exists in this class of materials. For most of the bimetallic complexes reported thus far, the resultant charge transfer [(4f)^{14}-(π*)^0-(4f)^{14} → (4f)^{13}-(π*)^2-(4f)^{13}] stems from the fact that each formally f^{14}/Yb^{II} metal center transfers an electron into the lowest unoccupied molecular orbital (LUMO) of the coordinated polypyridyl ligand to provide complexes that display properties consistent with two oxidized (f^{13}) metal centers

* To whom correspondence should be addressed. E-mail: kjohn@lanl.gov (K.D.J.), demorris@lanl.gov (D.E.M.).
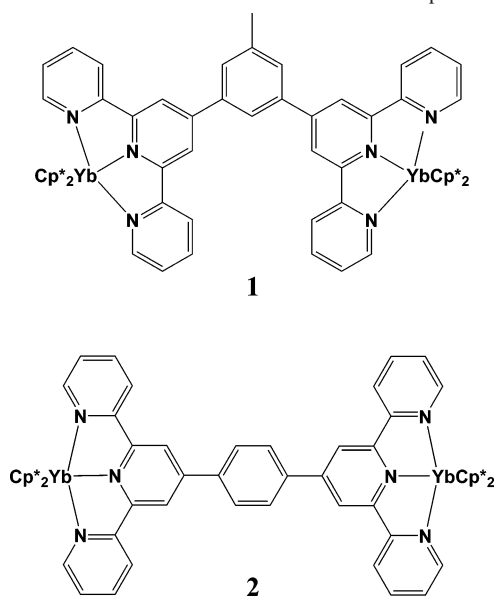† Chemistry Division.
‡ Theory Division.
§ Materials Physics Applications Division.

(1) Da Re, R. E.; Kuehl, C. J.; Brown, M. G.; Rocha, R. C.; Bauer, E. D.; John, K. D.; Morris, D. E.; Shreve, A. P.; Sarrao, J. L. *Inorg. Chem.* **2003**, *42*, 5551−5559.
(2) (a) Schultz, M.; Boncella, J. M.; Berg, D. J.; Tilley, T. D.; Andersen, R. A. *Organometallics* **2002**, *21*, 460−472. (b) Walter, M. D.; Schultz, M.; Andersen, R. A. *New J. Chem.* **2006**, *30*, 238−246.
(3) Veauthier, J. M.; Schelter, E. J.; Kuehl, C. J.; Clark, A. E.; Scott, B. L.; Morris, D. E.; Martin, R. L.; Thompson, J. D.; Kiplinger, J. L.; John, K. D. *Inorg. Chem.* **2005**, *44*, 5911−5920.

(4) Berg, D. J.; Boncella, J. M.; Andersen, R. A. *Organometallics* **2002**, *21*, 4622−4631.
(5) Carlson, C. N.; Kuehl, C. J.; Da Re, R. E.; Veauthier, J. M.; Schelter, E. J.; Milligan, A. E.; Scott, B. L.; Bauer, E. D.; Thompson, J. D.; Morris, D. E.; John, K. D. *J. Am. Chem. Soc.* **2006**, *128*, 7230−7241.
(6) Kuehl, C. J.; Da Re, R. E.; Scott, B. L.; Morris, D. E.; John, K. D. *Chem. Commun.* **2003**, 2336−2337.

Chart 1. Linear and Bent Bimetallic Ytterbocene Complexes **1** and **2**

been found to exist with a singlet-dianion bridging ligand [BL(αβ); BL = bridging ligand] ground state based upon spectroscopic evidence.[5] The singlet-dianion electronic configuration associated with **2** leads to antiferromagetic ordering of the metal spin carriers at ~10 K. This contrasts with the behavior of the 1,4-(2,2′-bipyridyl)benzene analog described above and sets the stage for a broader comparison of the roles of molecular symmetry and torsional distortions in determining the existence and relative magnitudes of electronic and magnetic coupling in these closely related families of linkage isomers of bimetallic ytterbocene complexes of polypyridyl chelators.

Experimental Section

Syntheses. All of the reactions and product manipulations were carried out under an atmosphere of dry argon or helium using standard dry box or Schlenk techniques. Anhydrous solvents, tetrahydrofuran (THF), toluene, diethyl ether, and methylene chloride were purchased from Aldrich or Acros and stored in the glovebox over activated 4 Å molecular sieves overnight and passed the sodium benzophenone ketyl test before use. $Cp^*_2Yb \cdot OEt_2$[10] and $[(Cp^*)_2Yb](1,4\text{-di(terpyridyl)benzene})[Yb(Cp^*)_2]$ (**2**)[5] were prepared according to the literature procedure. AgOTf was purchased from Aldrich and used as received. The ligand 1-methyl-3,5-bis-(2,2′:6′,2′′-terpyridin-4′-yl)benzene (1,3-dtb) was purchased from HetCat (www.hetcat.com) and used as received. Elemental analyses were performed by Midwest Microlabs, Indianapolis, IN.

$[(Cp^*)_2Yb]$(1-Methyl-3,5-bis(2,2′:6′,2′′-terpyridin-4′-yl)benzene)-$[Yb(Cp^*)_2]$ (1). A room-temperature toluene solution (5 mL) of $Cp^*_2Yb \cdot OEt_2$ (94.0 mg, 0.018 mmol) was added to solid 1-methyl-3,5-bis(2,2′:6′,2′′-terpyridin-4′-yl)benzene (50.3 mg, 0.009 mmol) with stirring. The solution immediately darkened and was stirred vigorously for 4 h. The toluene was removed under vacuum to yield a dark-green powder (131 mg, quantitative yield). The solid was recrystallized by slow evaporation of a concentrated THF solution to yield X-ray-quality green crystals. Anal. Calcd For $C_{77}H_{86}N_6$-Yb_2: C, 64.15; H, 6.01; N, 5.83. Found: C, 64.48; H, 6.13; N, 5.91. ^{1}H NMR (thf-d_8, δ): 105.74 (s, dtb), 3.81 (s, dtb), 2.12 (s, dtb), 1.29 (s, Me), −0.40 (C_5Me_5), −2.35 (s, dtb), −6.49 (s, dtb), −15.60 (s, dtb), −48.21 (s, dtb).

$[(Cp^*)_2Yb]$(1-Methyl-3,5-bis(2,2′:6′,2′′-terpyridin-4′-yl)benzene)-$[Yb(Cp^*)_2][OTf]_2$ [1]$^{2+}$. A room-temperature THF solution (5 mL) of $[Cp^*_2Yb]_2$(1,3-dtb) (100 mg, 0.069 mmol) was added to solid AgOTf (36.0 mg, 0.13 mmol) with stirring in the dark. The solution was stirred vigorously overnight. The following day, the THF was removed under vacuum, and the resulting powder was taken up into CH_2Cl_2 and filtered to yield an orange powder (94.2 mg, 78% yield). Anal. Calcd for $C_{79}H_{86}F_6N_6O_6S_2Yb_2 \cdot CH_2Cl_2$: C, 52.65; H, 4.86; N, 4.60. Found: C, 52.30; H, 4.83; N, 4.34. ^{1}H NMR (CD_2-Cl_2, δ): 72.03 (s, dtb), 30.39 (s, dtb), 27.13 (s, dtb), 23.15 (s, dtb), 21.30 (s, dtb), 18.29 (s, dtb), 17.46 (s, dtb), 8.24 (s, Me), −1.56 (C_5Me_5).

X-ray Diffraction. A crystal of **1** was mounted in a nylon cryoloop from Paratone-N oil under argon gas flow. The data were collected on a Bruker D8 APEX II charge-coupled-device (CCD) diffractometer with a KRYO-FLEX liquid nitrogen vapor cooling device. The instrument was equipped with a graphite monochromatized Mo Kα X-ray source ($λ = 0.71073$ Å), with MonoCap

and a bridging-ligand dianion. One new class of bimetallic complexes of the type $[Cp^*_2Yb]_2(1\text{-}^tBu\text{-}3,5\text{-}(2,2′\text{-bipyridyl})\text{-}C_6H_4)$ and $[Cp^*_2Yb]_2(1,4\text{-}(2,2′\text{-bipyridyl})\text{-}C_6H_4)$ ($Cp^* = C_5$-Me_5) and their corresponding two-electron oxidation products have recently been reported.[7] On the basis of established spin-coupling considerations,[8,9] it was anticipated that the 1,3-geometry would promote ferromagnetic coupling of the spins across the phenyl linker on the diradical ligand bridge with potential longer-range concerted coupling of the metal-based spin carriers as well. In contrast, the 1,4-geometry was expected to promote antiferromagnetic coupling of the diradical spins.[8,9] Although these new bimetallic systems were determined to possess diradical bridging ligands (i.e., ground-state electronic configuration $(4f)^{13}\text{-}(\pi^*)_A^1(\pi^*)_B^1$-$(4f)^{13})$, magnetic susceptibility measurements indicate that in both cases the exchange coupling mediated by the bis-2,2′-bipyridyl ligands is quite small and dominated by metal−ligand radical interactions similar to those seen in the monometallic systems with a $(4f)^{13}(\pi^*)^1$ electronic configuration. It was our conclusion that the overall low symmetry of these complexes as a result of the conformation of the phenyl bridge relative to the bpy rings and the potential for torsional distortions about the bpy-C_6H_4 bonds predisposed them to spin localization on the bpy orbital framework leading to inhibition of the expected magnetic interactions.

In our continuing pursuit of synthetic control of the electronic and magnetic coupling in bimetallic ytterbocenes, the present study reports the application of the ligand 1-methyl-3,5-bis(2,2′:6′,2′′-terpyridin-4′-yl)benzene (1,3-dtb) toward the synthesis of $[(Cp^*)_2Yb]$(1-methyl-3,5-bis(2,2′:6′,2′′-terpyridin-4′-yl)benzene)$[Yb(Cp^*)_2]$ (**1**, Chart 1). The 1,4-bis(terpyridyl)benzene (1,4-dtb) analog $[(Cp^*)_2Yb]$(1,4-di(terpyridyl)-benzene)$[Yb(Cp^*)_2]$ (**2**, Chart 1) has already

(7) Carlson, C. N.; Kuehl, C. J.; Ogallo, L.; Shultz, D. A.; Thompson, J. D.; Kirk, M. L.; John, K. D.; Morris, D. E. Submitted to *Organometallics*.
(8) Franzen, S.; Shultz, D. A. *J. Phys. Chem. A* **2003**, *107*, 4292−4299.
(9) Rajca, A. *Chem. Rev.* **1994**, *94*, 871−893.

(10) Tilley, T. D.; Boncella, J. M.; Berg, D. J.; Burns, C. J.; Andersen, R. A. *Inorg. Synth.* **1990**, *27*, 146.

Table 1. Crystal Data and Structure Refinement Parameters for **1**

	1
empirical formula	$C_{77} H_{86} N_6 Yb_2$
fw	1441.65
cryst syst	triclinic
No.	$P\bar{1}$
a, (Å)	15.2508(17)
b, (Å)	16.4829(19)
c, (Å)	17.400(2)
α, (deg)	70.861(1)
β, (deg)	85.484(1)
γ, (deg)	70.859(1)
V, (Å^3)	3901.6(8)
Z	2
D_{calcd}, (mg/m^3)	1.350
abs coef., (mm^{-1})	2.431
$F(000)$	1620
θ for data collection	1.24−25.49
limiting indices	$-18 \leq h \leq 18$
	$-19 \leq k \leq 19$
	$-21 \leq l \leq 21$
reflns	39 723
independent reflns	14 407 [R(int) = 0.0586]
completeness to $2q = 50.00°$	99.6%
refinement method	full matrix
	least-squares on F^2
data/restraints/params	14 407/0/478
GOF on F^2	1.134
final R indices [$I > 2\sigma$I]	R1 = 0.0667, wR = 0.1821
R (indices, all data)	R1 = 0.0904, wR2 = 0.1947
largest diff. peak and hole	2.041 and −2.398 e. Å^{-3}

Table 2. Selected Bond Lengths (Å) and Angles (deg) for **1**[a]

	1
Bond Lengths	
Yb−N$_{mean}$	2.391[8]
Yb−N$_{central}$	2.334[7]
Yb−N$_{terminal}$	2.419[8]
Yb−Yb	13.674(1)
Yb−Cp*$_{cent}$	2.48[1]
Bond Angles	
Cp*$_{cent}$−Yb−Cp*$_{cent}$ (av)	137.2[1]
C$_{pyr}$−C$_{pyz}$−C$_{Ar}$−C$_{Ar}$ (av)	33.5[1]
N$_{pyr}$−C$_{pyr}$−C$_{pyz}$−N$_{pyz}$ (av)	4.1[1]

[a] Esd's (standard deviations) are given in parentheses. Values in square brackets are arithmetic means of esd's.

X-ray source optics. A hemisphere of data was collected using ω scans with 5-second frame exposures and 0.3° frame widths. Data collection, initial indexing, and cell refinement were handled using APEX II[11] software. Frame integration, including Lorentz-polarization corrections, and final cell parameter calculations were carried out using SAINT+[12] software. The data were corrected for absorption using the SADABS[13] program. Decay of reflection intensity was monitored via analysis of redundant frames. The structure was solved using Direct methods and difference Fourier techniques. The electron density of four disordered thf molecules (237 e$^-$/cell and 1094 Å^3) was removed from the unit cell using PLATON/SQUEEZE.[14] The Cp* ligands of Yb(2) were disordered and were refined in two one-half occupancy positions. All of the hydrogen atom positions were idealized and rode on the atom to which they were attached. Hydrogen atom positions were not included on disordered atoms. The final refinement included anisotropic temperature factors on all of the non-hydrogen atoms. Structure solution, refinement, graphics, and creation of publication materials were performed using SHELXTL.[15] The crystal and refinement parameters for **1** are listed in Table 1. Selected bond distances and angles for **1** are provided in Table 2.

Magnetic Susceptibility. Magnetic measurements over the temperature range of 2−350 K were made using a Quantum Design superconducting quantum interference device (SQUID) magnetometer. The microcrystalline samples were sealed in borosilicate NMR tubes along with a small amount of quartz wool, which held the sample near the tube center. Contributions to the magnetization from the quartz wool and the tube were measured independently and subtracted from the total measured signal. The magnetic susceptibility, defined as the sample magnetization M divided by the applied magnetic field H, was measured as a function of temperature at an applied field of 0.1 T. Diamagnetic corrections were made using Pascal's constants.

Electrochemistry. Cyclic voltammetric studies were conducted in an inert nitrogen atmosphere glove box using a Perkin-Elmer Princeton Applied Research Corporation (PARC) Model 263 potentiostat under computer control using M270 software. The electrochemical cell was comprised of a modified PARC microcell consisting of a ~3 mm platinum disc working electrode, a Pt wire counter electrode, and a silver wire quasi-reference electrode. All of the experiments were conducted in purified THF using ~0.1 M $[(n\text{-}C_4H_9)_4N][B(C_6F_5)_4]$ as the supporting electrolyte. The benefits of this electrolyte for reducing uncompensated resistance in low dielectric solvents such as THF have been previously described.[16] Measured potentials were calibrated using the ferrocene/ferrocenium couple. Data were analyzed using the IGOR Pro (Wavemetrics, Inc.) software package on a Macintosh platform.

Electronic Absorption Spectroscopy. Electronic absorption spectra from ~200 to 1600 nm were recorded at room temperature using a Perkin-Elmer Lambda 19 or Lambda 950 spectrophotometer. Spectra were obtained in anhydrous THF against a solvent blank using 1 cm path-length quartz cells. Typical slit widths were 2 nm in the UV−visible range and 5−10 nm in the NIR range.

Computational Methods. Calculations were carried out for neutral and doubly reduced ligands 1,3-bis(2,2′:6′,2″-terpyridin-4′-yl)benzene (the methyl group has not been included for simplicity) and 1,4-bis(2,2′:6′,2″-terpyridin-4′-yl)benzene using the program Gaussian 03 (v. D.02)[17] utilizing the B3LYP hybrid density functional approach.[18,19] The 6-31G*(6d) basis set was used for all

(11) *APEX II 1.08*; Bruker AXS, Inc.: Madison, WI, 2004.

(12) *SAINT+ 7.06*; Bruker AXS, Inc.: Madison, WI, 2003.

(13) *SADABS 2.03*; George Sheldrick: University of Göttingen, Germany, 2001.

(14) Spek, A. L. *Acta Cryst.* **1990**, *A46*, C34.

(15) *SHELXTL 5.10*; Bruker AXS, Inc.: Madison, WI, 1997.

(16) (a) LeSuer, R. J.; Geiger, W. E. *Angew. Chem., Int. Ed.* **2000**, *39*, 248. (b) Camire, N.; Mueller-Westerhoff, U. T.; Geiger, W. E. *J. Organomet. Chem.* **2001**, *637−639*, 823.

(17) Frisch, M. J.; Trucks, G. W.; Schlegel, H. B.; Scuseria, G. E.; Robb, M. A.; Cheeseman, J. R.; Montgomery, J. A., Jr.; Vreven, T.; Kudin, K. N.; Burant, J. C.; Millam, J. M.; Iyengar, S. S.; Tomasi, J.; Barone, V.; Mennucci, B.; Cossi, M.; Scalmani, G.; Rega, N.; Petersson, G. A.; Nakatsuji, H.; Hada, M.; Ehara, M.; Toyota, K.; Fukuda, R.; Hasegawa, J.; Ishida, M.; Nakajima, T.; Honda, Y.; Kitao, O.; Nakai, H.; Klene, M.; Li, X.; Knox, J. E.; Hratchian, H. P.; Cross, J. B.; Bakken, V.; Adamo, C.; Jaramillo, J.; Gomperts, R.; Stratmann, R. E.; Yazyev, O.; Austin, A. J.; Cammi, R.; Pomelli, C.; Ochterski, J. W.; Ayala, P. Y.; Morokuma, K.; Voth, G. A.; Salvador, P.; Dannenberg, J. J.; Zakrzewski, V. G.; Dapprich, S.; Daniels, A. D.; Strain, M. C.; Farkas, O.; Malick, D. K.; Rabuck, A. D.; Raghavachari, K.; Foresman, J. B.; Ortiz, J. V.; Cui, Q.; Baboul, A. G.; Clifford, S.; Cioslowski, J.; Stefanov, B. B.; Liu, G.; Liashenko, A.; Piskorz, P.; Komaromi, I.; Martin, R. L.; Fox, D. J.; Keith, T.; Al-Laham, M. A.; Peng, C. Y.; Nanayakkara, A.; Challacombe, M.; Gill, P. M. W.; Johnson, B.; Chen, W.; Wong, M. W.; Gonzalez, C.; Pople, J. A. *Gaussian 03*, revision D.02; Gaussian, Inc.: Wallingford, CT, 2004.

(18) Lee, C.; Yang, W.; Parr, R. G. *Phys. Rev. B* **1988**, *37*, 785.

(19) Becke, A. D. *J. Chem. Phys.* **1993**, *98*, 5648−5652.
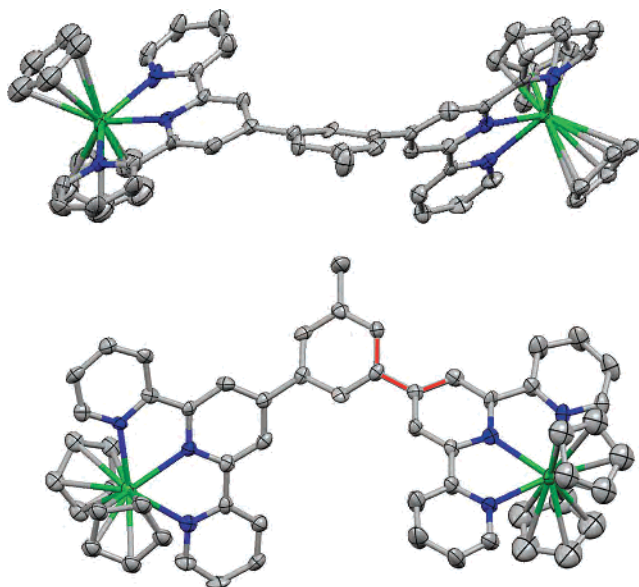
Figure 1. Thermal ellipsoid representation of **1** at the 50% probability level (side and top view). H atoms and Cp* methyl groups have been omitted for clarity. The $C_{pyr}-C_{pyr}-C_{Ar}-C_{Ar}$ torsion angle is shown in red for clarity.

of the C, H, and N atoms.[20] The neutral ligand geometries were optimized, and the relative energies of the singlet-dianion, singlet-diradical, and triplet-diradical electronic configurations were determined at that geometry.

Results and Discussion

Synthesis and Structure. 1 was prepared by the reaction of 2 equiv of Cp*$_2$Yb(Et$_2$O)[10] with 1 equiv of 1-methyl-3,5-bis(2,2′:6′,2″-terpyridin-4′-yl)benzene to yield a dark-green powder in quantitative yield. ^{1}H NMR supports the expected charge-transfer configuration, given the large chemical-shift window (-48 to 106 ppm). The dicationic form of [**1**]$^{2+}$ can be chemically isolated via addition of 2 equiv of AgOTf to provide an orange powder. Both complexes display ^{1}H NMR spectra that are indicative of highly symmetric complexes consistent with free rotation about the tpy-aryl bonds.

The structure of **1** is presented in Figure 1. To the best of our knowledge, this structure represents the first case of a 2:1 metal-to-ligand adduct of the 1,3-dtb framework.[21] In fact, it represents the second reported case of a structurally characterized 1,3-bis(polypridyl) complex; the other being a trinuclear copper(I)-bipyridine-based complex.[22] One of the key features of the structure of **1** is that both tpy moieties bind to the ytterbium in a tridentate manner with an average Yb—N distance of 2.391[8] Å and an average Yb—Cp*$_{centroid}$ distance of 2.48[1] Å. Both values are statistically indistinguishable from the previously reported monometallic analog Cp*$_2$Yb(tpy) (**3**) with Yb—N(ave) and Yb—Cp*$_{centroid}$ distances of 2.42[1] and 2.44[1] Å, respectively. The two tpy

groups are torsionally rotated out of the plane defined by the tolyl spacer by 26 and 41°, respectively. The angle separating the planes defined by the tpy moieties is 56°. The Yb—Yb distance is 13.7 Å. Single-crystal structural data are not available for **2** for comparison. However, the average Yb—Yb distance is 15.4 Å for the three reported transition-metal complexes employing the 1,4-dtb ligand.[23]

Computational Chemistry. DFT calculations were performed on the bridging ligands 1,3-bis(2,2′:6′,2″-terpyridin-4′-yl)benzene (1,3-dtb) and 1,4-bis(2,2′:6′,2″-terpyridin-4′-yl)benzene (1,4-dtb) with the aim of determining the relative energies of the lowest singlet and triplet states associated with the doubly reduced form of the bridging ligand. For the singlet state, we investigate two approximations. The first is the usual closed-shell singlet dianion. The second reflects the fact that we suspect singlet-diradical character in some of these states, and so the closed-shell spin equivalence restriction was removed and spin-unrestricted singlet-diradical solutions were investigated. In the case of the 1,3-dtb ligand, a broken-symmetry singlet-diradical solution lies lowest, with the corresponding triplet only 0.68 kcal higher in energy. The closed-shell singlet solution is well separated (8.55 kcal) from the diradical. In the case of the 1,4-dtb ligand, a singlet diradical is also lowest with the triplet diradical 1.41 kcal higher. Here, the energy stabilization associated with the diradical character is somewhat weaker, and the closed-shell singlet lies 5.01 kcal higher in energy. The natural orbitals describing the unpaired spin for the singlet diradical in 1,3-dtb and 1,4-dtb are presented in Figure 2. The 1,3-dtb ligand is well described as a singlet diradical, with the respective natural orbital occupation numbers being 1.1 and 0.9. However, the ground state of the 1,4-dtb ligand has considerably more closed-shell character as reflected in the occupation numbers of 1.34 and 0.66.

The DFT result for the 1,3-dtb ligand is somewhat surprising in that a triplet ground state might be expected on the basis of a number of previous theoretical treatments of spin coupling in 1,3-substituted phenylene dianions.[8,9,24] Note, however, that the energy difference of 0.68 kcal/mol separating the singlet- and triplet-diradical electronic states is small, and our calculations are designed as computational experiments as opposed to quantitative investigations; for example, our energies refer to differences in the geometry of the neutral ligand as opposed to that appropriate to each state. Geometry relaxation could certainly modify the energy by a few kcal/mol as could inclusion of the Yb moiety to which the ligand is bound.

It is also interesting that a singlet diradical electronic configuration lies lowest for the 1,4-derivative, even though

(20) Hehre, W. J.; Ditchfield, R.; Pople, J. A. *J. Chem. Phys.* **1972**, *56*, 2257−2261.

(21) Bruno, I. J.; Cole, J. C.; Edgington, P. R.; Kessler, M.; Macrae, C. F.; McCabe, P.; Pearson, J.; Taylor, R. *ConQuest: New Software for Searching the Cambridge Structural Database and Visualizing Crystal Structures.*, version 1.8; *Acta Crystallogr.* **2002**, *B58*, 389.

(22) Wood, C. R.; Benaglia, M.; Toyota, S.; Hardcastle, K.; Siegel, J. S. *Angew. Chem., Int. Ed.* **2001**, *40*, 749−751.

(23) (a) Koo, B.-K.; Bewley, L.; Golub, V.; Rarig, R. S.; Burkholder, E.; O'Connor, C. J.; Zubieta, J. *Inorg. Chim. Acta* **2003**, *351*, 167. (b) Maekawa, M.; Minematsu, T.; Konaka, H.; Sugimoto, K.; Kuroda-Sowa, T.; Suenaga, Y.; Munakata, M. *Inorg. Chim. Acta* **2004**, *357*, 3456. (c) Schmittel, M.; Kalsani, V.; Kishore, R. S. K.; Colfen, H.; Bats, J. W. *J. Am. Chem. Soc.* **2005**, *127*, 11544.

(24) (a) Shultz, D. A. *Magnetism: Molecules to Materials II: Molecule-Based Materials*; Wiley-VCH: Weinheim, Germany, 2002. (b) Shultz, D. A.; Fico, R. M.; Bodnar, S. H.; Kumar, R. K.; Vostrikova, K. E.; Kampf, J. W.; Boyle, P. D. *J. Am. Chem. Soc.* **2003**, *125*, 11761− 11771.

A

B
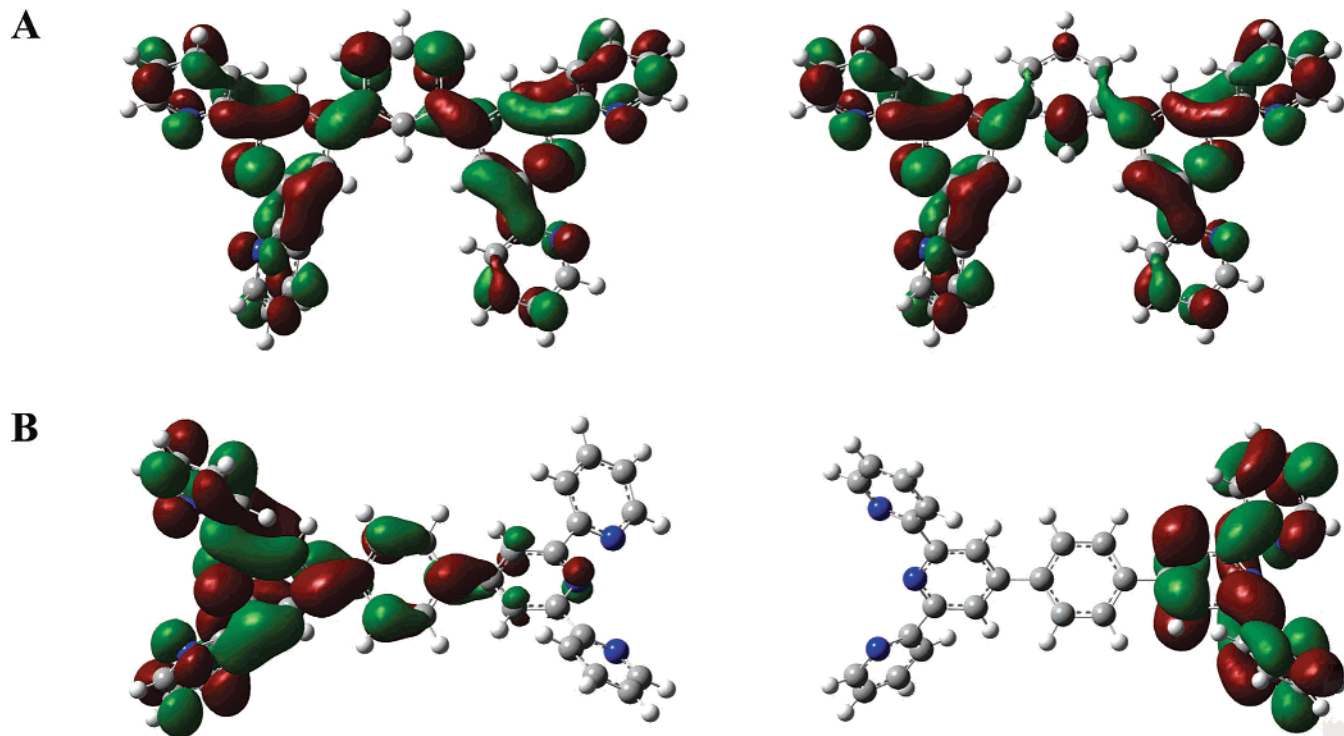
Figure 2. Natural orbitals with an occupation number equal to unity for the singlet diradicals of (A) 1,3-bis(2,2′:6′,2″-terpyridin-4′-yl)benzene and (B) 1,4-bis(2,2′:6′,2″-terpyridin-4′-yl)benzene calculated at the B3LYP/6-31G* level.

the symmetry breaking is weaker than in the 1,3 case. Examination of the calculated 1,4-dtb neutral ligand geometry reveals a significant $C_{pyr}-C_{pyr}-C_{Ar}-C_{Ar}$ torsion angle about the tpy−aryl bond of 38°. This torsional distortion serves to prevent electronic communication across the bridging aryl group, thus favoring a diradical as opposed to the closed-shell dianion. Given the fact that the spectroscopic characterization of **2** is most consistent with a closed-shell bridging dianion and that the natural orbital description implies more closed-shell character in the 1,4-dtb ligand, additional calculations were undertaken to investigate the role of the $C_{pyr}-C_{pyr}-C_{Ar}-C_{Ar}$ torsion angle on the nature of the lowest-energy state. It was found that a planar 1,4-dtb geometry still admitted a broken-symmetry diradical. However, the closed-shell dianion now lies only 1.45 kcal/mol above the broken-symmetry state, and the triplet is some 6.70 kcal higher in energy. The natural orbitals of the planar diradical ground state are characterized by occupation numbers of 1.64 and 0.36, confirming the greater closed-shell character in the singlet. These results suggest that the isolated 1,4-dtb dianion is best thought of in an intermediate coupling regime, with a ground state midway between the closed-shell dianion and the strongly localized diradical. Stated differently, one may think of the 1,4-dtb ground state as diradical in character but with a significant overlap between the orbitals containing the unpaired spin, whereas the unpaired spin occupies nearly orthogonal orbitals in the 1,3 derivative.

Electrochemistry. Room-temperature voltammetric data for the free ligands, the ytterbocene precursor $Cp*_2Yb(THF)_n$, and neutral complexes **1**−**3** in 0.1 M [(n-C$_4$H$_9$)$_4$N][B(C$_6$F$_5$)$_4$]/ THF are presented in Figure 3. Metrical data extracted from these voltammograms are summarized in Table 3. The data

for **2** and **3** have been reported by us previously[3,5,6] but are reproduced here for comparison. The reversible oxidation wave for the ytterbocene THF adduct is attributed to the one-electron oxidation of the ytterbium metal center, $4f^{14} \rightarrow 4f,^{13}$ as noted previously.[1] The data demonstrate that the ytterbocene THF precursor has insufficient thermodynamic driving force to reduce the free ligands in the absence of coordination. However, upon complexation, there are significant shifts in the potentials of the voltammetric waves in the system. Shifts in the redox potentials of both metal-based and ligand-based couples upon coordination are common and provide a direct measure of the perturbations in orbital energies as a result of the complex formation. Note that in the uncomplexed form both bridging terpyridyl-based ligands (1,3-dtb and 1,4-dtb) exhibit multiple reversible reduction waves within the available potential window of this solvent/supporting electrolyte system. These reduction processes in the free ligands are clearly associated with successive one-electron additions into the low-lying π^* orbital(s). However, it is unclear in these cases whether the first two electrons enter the same orbital (delocalized over the entire ligand framework) to give $(\pi^*)^1$ and $(\pi^*)^2$ electronic configurations, respectively, or whether there are two nearly degenerate low-lying π^* orbitals (due, for example, to disruption of an extended π^* orbital from torsions about the bridging phenyl group) that each accept one electron.

The spacing between the first two reduction waves for 1,3-dtb and 1,4-dtb are similar (Table 3), suggesting a comparable orbital disposition of the two electrons in both ligands. However, the spacings are significantly smaller (190 and 220 mV, respectively) than typical for the occupation of two
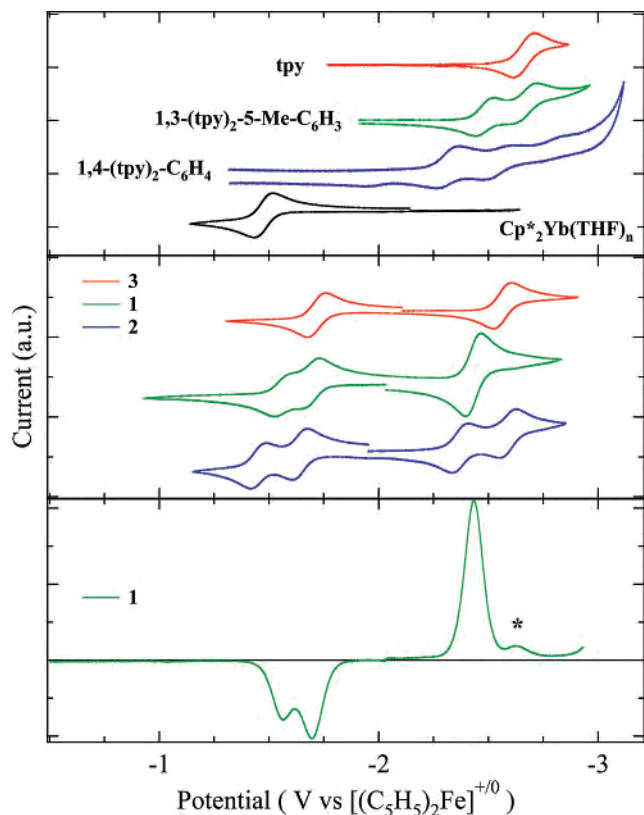
Figure 3. Voltammetric data at a Pt disk working electrode in 0.1 M [(n-C$_4$H$_9$)$_4$N][B(C$_6$F$_5$)$_4$]/THF at room temperature. Top panel: Cyclic voltammograms for complex precursors. Middle panel: Cyclic voltammograms for **1**–**3**. Bottom panel: Square wave voltammogram for **1** (see text). Cyclic scan rates were 200 mV/s. Square wave scan was at 60 Hz with a pulse height of 25 mV. Concentrations of all of the analytes were ~5 mM. Currents are in arbitrary units to facilitate comparisons. The small peak marked with an asterisk is due to a degradation product from the slow reaction of the complex with the electrolyte.

Table 3. Summary and Comparison of Redox Data^a Derived from Cyclic and/or Square-Wave Voltammetric Data for Ytterbocene Complexes

	ligand-based		metal-based	
	$E_{1/2}$ (L$_1$)	$E_{1/2}$ (L$_2$)	$E_{1/2}$ (M$_a$)	$E_{1/2}$ (M$_b$)
tpy^b	−2.66			
3^b	−1.72		−2.56	
1,4-dtb^b	−2.32	−2.54		
2^b	−1.45	−1.64	−2.37	−2.59
1,3-dtb	−2.48	−2.67		
1	−1.56	−1.70	−2.43	^{c}
	1,3-dtb	**1**	1,4-dtb	**2**	**3**
$|\Delta(E_{1/2})$ [M−L]$|$ ^{d}		0.73		0.73	0.84
$|\Delta(E_{1/2})$ [M$_a$−M$_b$]$|$		0.00		0.22	
$|\Delta(E_{1/2})$ [L$_1$−L$_2$]$|$	0.19	0.14	0.22	0.19	

^{a} All of the values are in volts. $E_{1/2}$ values are versus [(C$_5$H$_5$)$_2$Fe]$^{+/0}$ in 0.1 M [(n-C$_4$H$_9$)$_4$N][B(C$_6$F$_5$)$_4$]/THF at room temperature. ^{b} Data from ref 5. ^{c} Only one 2 e$^-$ metal-based reduction wave was observed (see text). ^{d} Separation in $E_{1/2}$ values between the most positive metal-based reduction wave and the most negative ligand-based oxidation wave.

electrons in the same π^* orbital (i.e., the ligand-dianion configuration) because in this case the spacing is a rough approximation of the orbital spin-pairing energy and is typically closer to ~1 V.[25] The DFT result described above suggests that the diradical state is the lowest for both of these ligands. Thus, the interpretation of the voltammetric data that

(25) Vlcek, A. A. *Coord. Chem. Rev.* **1982**, *43*, 39−62.

would be the most consistent with this theoretical result would be to have each of the first two added electrons entering one of two nearly degenerate orbitals, with the interaction between the electrons in these orbitals (as measured by the spacing of the voltammetric waves) being slightly larger in the 1,4-dtb ligand than in the 1,3-dtb ligand.

A comparison of the voltammetric data for **1** and **2** is where we clearly begin to see the differences in the properties of these bimetallic complexes. We have previously assigned the reversible voltammetric waves for **2** and **3** seen in the potential region illustrated in Figure 3.[1,3,5,6] Specifically, for **3** the voltammetric waves are ascribed to a metal-based one-electron reduction step (4f^{13} → 4f^{14}) and a ligand-based one-electron oxidation step (tpy$^{•-}$ → tpy^0). Similarly, the voltammetric waves for **2** in Figure 3 can be ascribed to two successive one-electron oxidations of the bridging ligand and a one-electron reduction of each of the two ytterbium metal centers. This same general pattern was exhibited by all of the tpy-based bimetallic complexes reported previously,[5] although the spacings between the waves were substantially larger for some of the tpy-based bimetallic complexes, reflecting greater interactions among the redox centers. **1** also exhibits two reversible, ligand-based oxidation waves. However, the most notable feature in the voltammetric properties of **1** relative to *all* of the other bimetallic ytterbocene complexes we have investigated is that only a single metal-based reduction wave is observed in this potential region.[26]

To characterize more fully the properties of this single, reversible reduction wave seen for **1**, square-wave voltammetric data were obtained. These results are illustrated in the bottom panel of Figure 3. These data much more clearly illustrate two important factors: (1) the voltammetric wave seen in the cyclic scan does not resolve into two waves under the greater resolution of a square-wave scan, and (2) the peak current in this single metal-based reduction wave is almost exactly twice the peak current found in the first (most-negative) ligand-based oxidation wave. This is prima facie evidence that the metal-based reduction wave involves the simultaneous transfer of two electrons (i.e., each metal center is reduced by one electron at the same potential). To ascertain whether this two-electron reduction is a concerted two-electron process or simply the transfer of one electron onto each metal center at the same potential, the scan-rate dependence of the cyclic voltammetric peak currents was examined. Recall that there is a well-defined relationship between the peak current in a voltammetric wave and the number of electrons involved in the process: $i_{pk} \propto (\nu^{1/2})(n^{3/2})$ where ν is the scan rate (V/s) and n is the number of electrons involved in the redox step.[27] Furthermore, voltammetric currents are additive for processes occurring at the same potential. Thus, a concerted two-electron step should exhibit

(26) As with all other ytterbocene polypyridyl adducts we have investigated, there are other irreversible voltammetric waves observed at potentials near the negative limit of the solvent/supporting electrolyte (~ −3 V) that are attributed to further reductions of the bridging ligand. Likewise, oxidative electrochemistry attributed to the Cp* rings can be seen at ~1 V in all of these systems.

(27) Bard, A. J.; Faulkner, L. R. *Electrochemical Methods: Fundamentals and Applications*; John Wiley and Sons: New York, 2001.
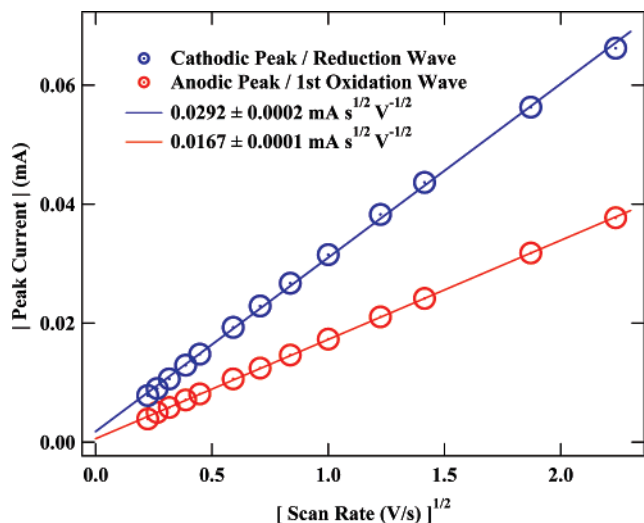
Figure 4. Scan-rate dependence of the peak currents for the sole reduction wave and the first (most-negative) oxidation wave in the cyclic voltammetric data for **1** at a Pt disk working electrode in 0.1 M $[(n\text{-}C_4H_9)_4N][B(C_6F_5)_4]$/ THF at room temperature. Slopes indicated for the lines were determined by linear least-squares fits to all of the data points. Correlation coefficients (*R*) were 0.9996 and 0.9999 for the cathodic and anodic peak data, respectively.

a peak current versus $\nu^{1/2}$ with a slope that is $2^{3/2}$ ($\sim$2.8) times that of a one-electron step, whereas if the process involves the simple overlap in potential of two one-electron steps, the peak current versus $\nu^{1/2}$ should have a slope that is $1^{3/2} + 1^{3/2} = 2$ times that of a single one-electron step. The peak current data for **1** versus $\nu^{1/2}$ are illustrated in Figure 4 using the first (most-negative) ligand-based oxidation wave as the internal current standard for a one-electron transfer step. Note that the ratio of the slopes (1.75) of the line for the reduction step to that of the oxidation step is close to 2 and is clearly significantly less than the value of 2.8 expected for a comparison of a concerted two-electron transfer process to a one-electron process.[28] Thus, this reduction wave for **1** must correspond to the one-electron reduction of each Yb metal center that takes place at the same potential.

As we have noted in our previous reports, the potential separation between waves is one of the most important diagnostic aspects of these voltammetric data, because it provides direct information on the degree of electronic interaction between the metal centers and between each metal center and the bridging ligand. These data are summarized in Table 3. The most salient parameter to assess the electronic interactions is the potential separation between the waves associated with the metal-based processes ($\Delta(E_{1/2})(M_a-M_b)$ in Table 3). Whereas this metric has been shown recently to be sensitive to ion-pairing and solvation effects,[29] and can be varied significantly by changing the solvent/supporting electrolyte composition, we have kept the solvent/supporting electrolyte system (THF/$\sim$0.1 M $[(n\text{-}C_4H_9)_4N][B(C_6F_5)_4]$)

constant throughout the studies reported here and previously.[1,3,5,6] Thus, comparisons of $\Delta(E_{1/2})$ values among these ytterbocene complexes remain strictly valid and informative of *differences* in the extent of electronic communication in a relative sense among these systems. In the absence of any metal–metal interaction, the metal-based redox processes should occur at the same potential (i.e., two superimposed one-electron waves) with perhaps a slight, experimentally indiscernible offset ($\sim$36 mV) due to statistical (entropic) factors.[27] This is the exact behavior seen for the metal-based reduction in **1**, demonstrating that the electronic interaction between metals is essentially negligible. For comparison, the value for **2** is 220 mV, indicating some weak interaction between the metal centers, although still much less than the 600 mV separation seen for the tetra(2-pyridyl)pyrazine bridged bimetallic complex possessing a significantly shorter metal–metal separation.[5]

The separation between the bridging-ligand-based oxidation waves ($\Delta(E_{1/2})(L_1-L_2)$ in Table 3) for the bimetallic complexes should also convey information about the orbital disposition of and interaction between the ligand-based π^* electrons and, by comparison to the data for the free ligands, any structural and energetic perturbation(s) induced by the coordination of the $Cp^*_2Yb^{III}$ centers. However, these Δ-$(E_{1/2})(L_1-L_2)$ values remain remarkably consistent for **1**, **2**, and their corresponding free ligands. Whereas the observed differences are statistically significant with respect to the uncertainty in the measurements, they do not appear to reflect any substantial change in electronic configuration (e.g., a transition from a bridging-ligand diradical to a spin-paired dianion) or structural change (e.g., sterically induced torsional changes about the central phenyl group) that might be anticipated on the basis of other data (vide infra). These electrochemical oxidation data seem most consistent with a description of the bridging ligand as a discrete diradical with weakly interacting localized spins.

Optical Spectroscopy. The room-temperature UV–visible NIR electronic absorption spectral data for neutral complex **1** and dication $[1]^{2+}$ in THF are provided in Figure 5. Previously reported data for **2**, $[2]^{2+}$, **3**, and $[3]^{1+}$ are included for comparison.[5,6] Because of the large number of possible electronic transitions in both the neutral and cationic complexes, detailed band assignments of the observed optical transitions are outside of the scope of this effort. Instead we focus on a comparison of the spectral properties for **1**, **2**, and **3** and those of their respective (di)cations, particularly in relation to the behavior observed and reported previously for the bpy- and tpy-based bimetallic systems.[5−7]

Neutral Complexes. The similarities and hence the comparisons of the optical spectral data in the UV–visible NIR region for **1** relative to **2** or **3** (Figure 5, top panel) are less compelling than they have been in our previous comparative studies of these bimetallic ytterbocene com-
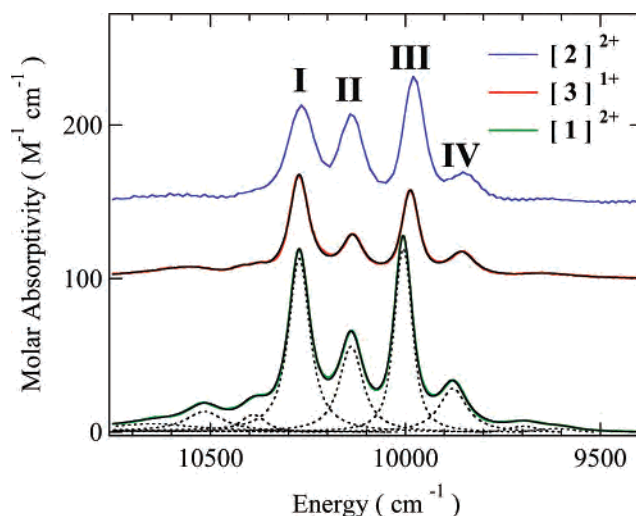
(28) The use of the peak current in the ligand-based oxidation wave as an internal standard in constructing Figure 3 eliminates uncertainties in complex concentration and electrode surface area, but there can still be differences in the diffusion coefficients for the oxidation versus reduction waves that could contribute to differences in the observed slopes. However, these are expected to be relatively small because both processes involve the diffusion of a neutral species of the identical hydrodynamic radius to the electrode surface.

(29) (a) Yeomans, B. D.; Kelso, L. S.; Tregloan, P. A.; Keene, F. R. *Eur. J. Inorg. Chem.* **2001**, 239−246. (b) Barriere, F.; Camire, N.; Geiger, W. E.; Mueller-Westerhoff, U. T.; Sanders, R. *J. Am. Chem. Soc.* **2002**, *124*, 7262−7263. (c) D'Alessandro, D. M.; Keene, F. R. *Dalton Trans.* **2004**, 3950−3954. (d) Barriere, F.; Geiger, W. E. *J. Am. Chem. Soc.* **2006**, *128*, 3980−3989.
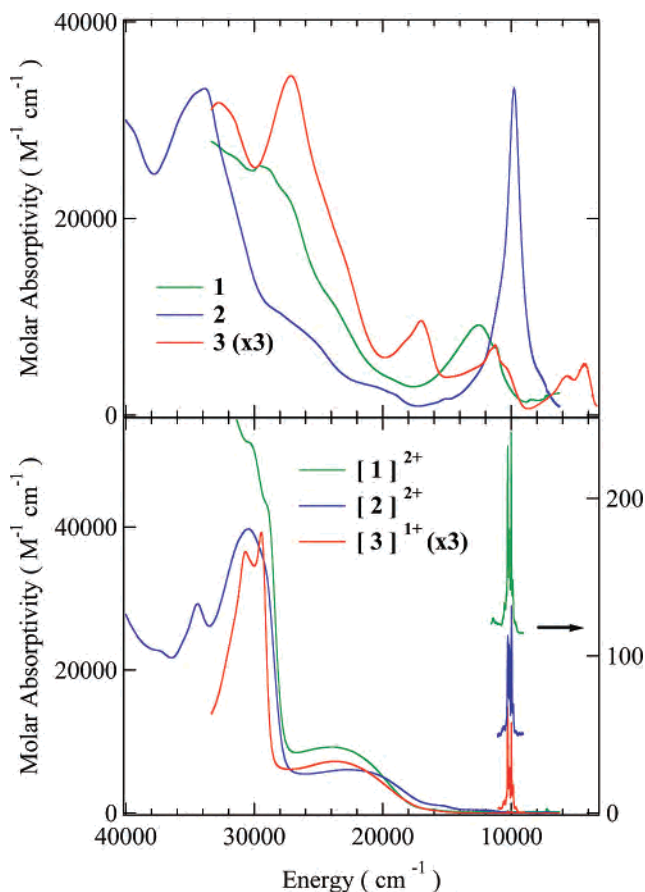
Figure 5. UV−vis NIR electronic absorption spectra at 300 K for neutral complexes in THF (top) and cationic complexes in CH₂Cl₂ ([2]²⁺ and [3]⁺) and THF ([1]²⁺) (bottom). The intensity scaling for [3]¹⁺ applies only to the UV−visible portion of the spectrum. NIR spectra in the bottom panel have been offset to facilitate comparison.

Figure 6. NIR spectral data for [1]²⁺ in THF and [2]²⁺ and [3]¹⁺ in CH₂-Cl₂ at 300 K. Results of spectral fitting using unconstrained Voigt functions are shown in solid black lines for [3]¹⁺ and [1]²⁺. Constituent bands from the fit for [1]²⁺ are shown in dashed lines. See text for details. Spectra have been offset to facilitate comparison.

plexes. There are two significant spectral observations that capture the differences between **1** and **2** and provide some definitive insight into assignment of the ground-state electronic configuration. First, the band energies and widths in the visible region for **1** are much more comparable to those for monometallic **3** than bimetallic **2**. In **3**, the principal bands at ∼17 000 and ∼11 000 cm⁻¹ have been attributed to tpy-ligand-based transitions derived from the open-shell radical anion configuration on the basis of observations of nearly identical bands in alkali-metal-reduced free tpy.[5] Second, for **2** this spectral region is dominated by a very intense, narrow band at ∼10 000 cm⁻¹ that has been assigned to a transition derived from the doubly reduced ligand dianion. This same transition has been observed as the dominant feature in all of the bis(tpy)-based bridging-ligand bimetallic complexes we have examined, and it appears to be the hallmark of the singlet-dianion bridging-ligand structure (i.e., $(\pi^*)^2$).[5] There is no evidence for this very diagnostic band in the spectrum of **1**. Thus, the closer similarity in spectral characteristics between **1** and **3** and the absence of the diagnostic transition associated with the singlet-dianion bridging ligand in the spectrum of **1** together argue in favor of a description of the electronic structure in **1** as two effectively independent $Cp^*_2Yb^{3+}(tpy^{-\bullet})$ moieties with a

net electronic configuration of $(4f)^{13}(\pi_A^*)^1(\pi_B^*)^1(4f)^{13}$ rather than the $(4f)^{13}(\pi^*)^2(4f)^{13}$ configuration proposed previously for **2**.

This description of the ground state in **1** is consistent with the electrochemical data described above in that there is no evidence from these spectral data for electronic coupling of the metal centers across the phenyl linker group. Unfortunately, the optical data for **1** (and **2**) show no evidence for the f−f electronic bands expected for systems containing Yb(III) ions. These bands should provide a key optical spectral diagnostic for electronic and/or magnetic coupling between the metal centers, but they are expected to lie at ∼10 000 cm⁻¹ (vide infra), and the comparatively low oscillator strengths derived from their parity forbidden character makes them indiscernible beneath the more intense ligand radical transitions that tail into this spectral window. As noted previously, these diagnostic bands have been absent from the spectra of nearly all of the neutral ytterbocene polypyridine adducts we have investigated.[1,3,5−7]

Cationic Complexes. The optical data for [1]²⁺, [2]²⁺, and [3]¹⁺ over the entire UV−vis NIR spectral range are provided in Figure 5, bottom panel. These spectral data are significantly simplified relative to the neutral complex data because these species no longer possess electrons in polypyridyl-based π^* orbitals that engender the intense transitions throughout the visible and NIR. In fact, the absence of ligand-based π^* electrons in these systems provides an optimal means to focus directly on the spectral manifestations of metal−metal interactions because the potential influence of singlet- or triplet-ligand diradicals versus singlet dianion on metal communication have been eliminated, leaving only the influences of metal−metal separation and ligand-based structural distortions to consider.

The assignments for the broad spectral bands in the visible region for [1]²⁺ are identical to those proposed previously for cationic monometallic and dicationic bimetallic ytter-

Table 4. Summary of f−f Transition Parameters from NIR Spectra of Cationic Ytterbocene Complexes[a,b]

	band I			band II			band III			band IV		
complex	peak energy (cm^{-1})	integrated intensity	fwhm (cm^{-1})	peak energy (cm^{-1})	integrated intensity	fwhm (cm^{-1})	peak energy (cm^{-1})	integrated intensity	fwhm (cm^{-1})	peak energy (cm^{-1})	integrated intensity	fwhm (cm^{-1})
[3]$^{+}$ [c]	10 273	6370	60	10 135	2510	67	9987	3950	51	9855	1930	83
[1]$^{2+}$	10 272	11 100	64	10 139	6110	72	10 006	9010	54	9878	3850	86
[2]$^{2+}$ [c]	10 267	6830	82	10 138	5090	72	9978	6710	63	9849	2030	90

[a] See Figure 5 for identification of the bands. [b] Integrated intensities are derived from the unconstrained Voigt profile fits of the spectra; see text for details. [c] These data are from ref 5.
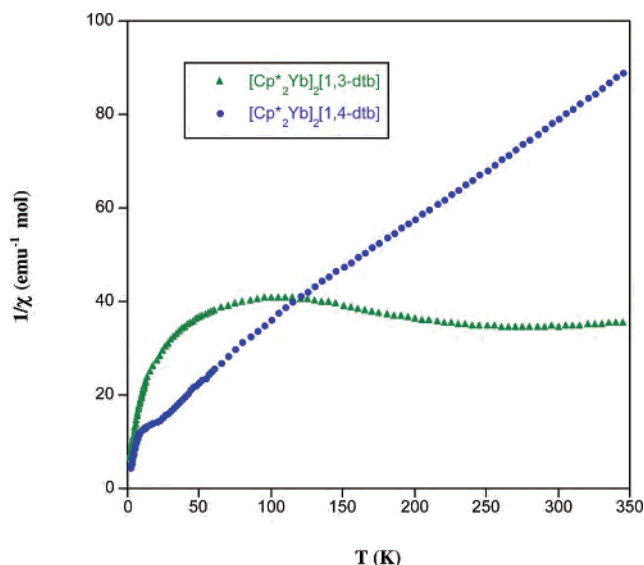
bocene complexes including **[2]**$^{2+}$ and **[3]**$^{1+}$.[1,3,5−7] Specifically, the higher-energy, more-intense band at ∼18 000−26 000 cm^{-1} is assigned to a polypyridyl ligand (π)-to-metal (4f) charge-transfer transition on the basis of detailed resonance Raman data for **[3]**$^{+}$ presented elsewhere[30] and by analogy to the spectrum of oxidized (d^5) transition-metal polypyridyl complexes (e.g., [Ru(bpy)$_3$]$^{3+}$).[31] The less intense band at ∼14 000−18 000 cm^{-1} is assigned to the related Cp* ligand (π)-to-metal (4f) charge-transfer transition(s). This assignment is based on comparison to the spectra of many structurally related monometallic ytterbocene complexes (e.g., Cp*$_3$Yb and Cp*$_3$Yb(L); L = THF, PEt$_3$, etc.).[32] As in the comparison of the spectra for the neutral complexes described above, there is again a very striking similarity in the spectral properties of **[1]**$^{2+}$ and **[3]**$^{1+}$ (except for intensity differences, vide infra) suggesting that the two Cp*$_2$Yb^{3+}-(tpy^0) moieties in **[1]**$^{2+}$ are electronically the same as that in **[3]**$^{1+}$ (i.e., there is no measurable metal−metal interaction in **[1]**$^{2+}$ to perturb the electronic transitions). The bands in this region for **[2]**$^{2+}$ are red shifted by ∼2000 cm^{-1} relative to the bands in **[1]**$^{2+}$. However, this red shift most likely reflects a change in the relative energy of the π orbitals of 1,4-dtb versus 1,3-dtb rather than an influence from metal−metal interaction.

The additional new feature in the spectrum of **[1]**$^{2+}$, as with all of the fully oxidized ytterbocene polypyridyl adducts investigated thus far, is the emergence of the f−f transitions deriving from the f^{13} electronic configuration on the two ytterbium centers (right-hand scale, Figure 6, bottom panel). As expected on the basis of data from other Yb(III) complexes, these bands are centered at ∼10 000 cm^{-1}, they are quite narrow, and they have much lower oscillator strengths consistent with the Laporte forbidden nature of the transitions. Figure 6 compares the principal f−f bands for **[1]**$^{2+}$, **[2]**$^{2+}$, and **[3]**$^{1+}$.

To quantify this comparison, the spectrum for **[1]**$^{2+}$ in this region was fit using Voigt functions[33] as described previously for these systems.[5,7] The fitting results are included in the traces in Figure 6, and the metrical results for each of the four principal spectral bands identified in Figure 6 are provided in Table 4 and compared to the fitting results reported previously for **[2]**$^{2+}$ and **[3]**$^{1+}$. Note in particular

that the peak positions of these four principal bands are strikingly similar for all three complexes, although there is some variation in the relative intensity pattern among these four bands in the three systems. Perhaps the most interesting observation is that the band intensities in these four bands for **[1]**$^{2+}$ are uniformly nearly two times those for **[3]**$^{1+}$ and retain the same approximate band widths. In contrast, as noted in our previous study of these dicationic bis(tpy) complexes,[5] these same bands in **[2]**$^{2+}$ appear significantly broader than those for **[3]**$^{1+}$ while also doubling in integrated intensity. This broadening was ascribed to a slight (unresolved) splitting of these bands, reflecting a weak coupling between the metal centers. The absence of broadening in the bands of **[1]**$^{2+}$ relative to those of **[3]**$^{1+}$ concomitant with the doubling in intensity is yet another manifestation of the complete uncoupling of the two metal centers in this new complex.

Magnetic Susceptibility. The magnetic susceptibility (χ) data for **1** and that for the previously reported **2** are presented in Figure 7. **2** displays Curie−Weiss law behavior to approximately 50 K. A weak feature at ∼10 K is observed that has been previously ascribed to an antiferromagnetic coupling effect of the type Yb(α)BL($\alpha\beta$)Yb(β).[5] The basis of the observed low-temperature magnetic coupling behavior is rooted in the observed electronic ground-state [(f)^{13}-(π*)^2-(f)^{13}] associated with **2**. The doubly occupied π* orbital of the associated bridging-ligand dianion facilitates magnetic coupling through a spin-polarization mechanism. **2** displays

(30) Da Re, R. E.; Kuehl, C. J.; Donohoe, R. J.; John, K. D.; Morris, D. E. *Electronic Spectroscopy of [(C$_5$Me$_5$)$_2$Yb(L)]$^+$ (L = 2,2′-bipyridine and 2,2′:6′,2′′-terpyridine). Vibronic Coupling and Ligand-Field Splitting in the 4f^{13}-Derived Ground and Excited States of Yb^{3+}*; Report LA-UR-05−5249; Los Alamos National Laboratory: Los Alamos, NM, 2005.

Figure 7. $1/\chi$ (△) versus T for (Cp*$_2$Yb)$_2$BL at 0.1 T. BL: Blue = 1,4-dtb; Green = 1,3-dtb.

a room-temperature magnetic moment of $5.70\mu_B$ that approaches the expected value of $6.4\mu_B$ for two uncoupled Yb^{III} ($^2F_{7/2}$) ions.

Like **2**, **1** displays a room-temperature moment ($5.9\mu_B$) approaching the value of two uncoupled Yb^{III} centers. Unlike **2**, **1** displays a temperature-dependent magnetic profile that departs dramatically from the Curie law. The observed temperature-dependent susceptibility profile for **1** is reminiscent of that previously reported for monometallic analogs of the type $Cp*_2Yb(L)$ (L = bpy, tpy, tpyCN).[2a,3] This monometallic-like behavior would suggest that the 1,3-geometry in **1** has inhibited magnetic coupling across the bridging ligand. This is unlike the case for the 1,4-geometry presented in **2** but similar to that seen for the bis-(bpy)-bridged systems reported recently.[7] Furthermore, this behavior is most consistent with the fact that the two ytterbocene/tpy moieties are behaving as independent magnetic units. Unfortunately, the magnetic data presented in this study do not provide an adequate enough description of the low-temperature magnetic behavior to indicate the type (if any) of spin coupling imposed by the diradical form of the 1,3-dtb bridging ligand. Given that **2** exhibits spin coupling at ∼10 K, it is our expectation that **1** should exhibit coupling that is at least a factor of 2 lower on the basis of ligand geometry considerations. Future magnetic analyses will focus on the application of magnetic circular dichrosism (MCD) to better study low-temperature magnetic coupling.

Summary and Conclusions

We have a prepared a novel bimetallic complex in which the bridging-ligand 1-methyl-3,5-bis(2,2′:6′,2″-terpyridin-4′-yl)benzene is designed to induce ferromagnetic coupling of the two Yb^{III} centers. The structure of **1** represents the first time a bimetallic complex has been structurally characterized with this ligand. This new ligand geometry in **1** has done an effective job of turning off all of the electronic communication between the metal centers in both neutral and dicationic speices as evidenced by the net two-electron reduction process associated with the Yb(III/II) couples for the neutral complex as compared to the process for two separate ($4f^{13} \rightarrow 4f^{14}$) couples previously reported for the 1,4-bis-(tpy) analog and the nearly exact doubling of the intensity in the f−f bands in the dicationic complex.

Magnetic susceptibility measurements on **1** indicate that the magnetic coupling of the type $Yb(\alpha)BL(\alpha\beta)Yb(\beta)$ exhibited by **2** has been prevented by the 1,3 geometry. Future studies will focus upon the low temperature (<20 K) magnetic behavior of **1** to determine the nature of the magnetic coupling using techniques like magnetic circular dichroism (MCD).

Supporting Information Available: Full crystallographic details for **1** are available (CCDC 617297), plots of χT vs T for complex [**1**]$^{2+}$ and complete ref 17. This material is available free of charge via the Internet at http://pubs.acs.org.

IC0702973

(31) (a) Bergkamp, M. A.; Gutlich, P.; Netzel, T. L.; Sutin, N. *J. Phys. Chem.* **1983**, *87*, 3877−3883. (b) Braterman, P. S.; Song, J. I.; Peacock, R. D. *Spectrochimica Acta, Part A* **1992**, *48*, 899−903. (c) Bryant, G. M.; Fergusson, J. E. *Aust. J. Chem.* **1971**, *24*, 275−286. (d) Nazeeruddin, M. K.; Zakeeruddin, S. M.; Kalyanasundaram, K. *J. Phys. Chem.* **1993**, *97*, 9607−9612.

(32) Schlesener, C. J.; Ellis, A. B. *Organometallics* **1983**, *2*, 529−534.

(33) Armstrong, B. H. *J. Quant. Spectrosc. Radiat. Transfer* **1967**, *7*, 61−88.

(34) (a) Kahn, M. L.; Sutter, J.−P.; Golhen, S.; Guionneau, P.; Ouahab, L.; Kahn, O.; Chasseau, D. *J. Am. Chem. Soc.* **2000**, *122*, 3413−3421. (b) Kahn, M. L.; Ballou, R.; Porcher, P.; Kahn, O.; Sutter, J.-P. *Chem.−Eur. J.* **2002**, *8*, 525−531. (c) Sutter, J.-P.; Kahn, M. L.; Golhen, S.; Ouahab, L.; Kahn, O. *Chem.−Eur. J.* **1998**, *4*, 571−576. (d) Kahn, M. L.; Ballou, R.; Porcher, P.; Kahn, O.; Sutter, J.-P. *Chemistry* **2002**, *8*, 525−531. (e) Benelli, C.; Gatteschi, D. *Chem. Rev.* **2002**, *102*, 2369−2387. (f) Benelli, C.; Caneschi, A.; Gatteschi, D.; Sessoli, R. *Inorg. Chem.* **1993**, *32*, 4797−801.

(35) Zhang, G.; Li, S.; Jiang, Y. *J. Phys. Chem. A* **2003**, *107*, 5573−5582.